

Small punch creep investigation of Eurofer97 and 14Cr oxide dispersion strengthened steel

M. Richardson^{*}, M. Gorley, Y. Wang, D. Andres, H. Dawson

UKAEA, Culham Science Centre, Abingdon, Oxfordshire OX14 3DB, UK

ARTICLE INFO

Keywords:

Small Punch Creep
Eurofer97
ODS Steel
14YWT
SSTT

ABSTRACT

Small punch creep (SPC) testing represents an effective way to rapidly assess the creep performance of novel materials and potentially monitor degradation of in-service components. Recent progress in standardisation has also led to improvements in data analysis. However, estimation of equivalent uniaxial stresses is still somewhat challenging and has hindered wider usage of the small punch technique. In this study, the creep properties of two candidate materials for structural applications in future fusion reactors were assessed via SPC. These included the baseline structural material, Eurofer97, and a more recently developed 14Cr Oxide Dispersion Strengthened (ODS) steel (14YWT). Having been assessed at 550 °C, the 14YWT demonstrated superior creep life and significantly lower rates of deformation, but also exhibited reduced ductility. The Modified Chakrabarty (MCH) approach was employed to estimate equivalent uniaxial creep stresses. This methodology appeared to work well with the Eurofer97 but struggled when applied to 14YWT, making accurate estimation of the 14YWT performance difficult. Since the MCH approach was developed for ductile materials, its predictive capabilities may have been limited by the low ductility of 14YWT.

Introduction

The prospect of delivering almost unlimited clean energy in a controlled manner makes nuclear fusion one of the most sought after goals in tackling climate change and the energy crisis [1]. However, the development of large scale fusion power plants represents one of the greatest engineering challenges facing humankind today [2]. The environment within a commercial fusion power plant reactor will be one of the most hostile imaginable, with materials exposed to high heat flux, neutron irradiation, plasma erosion, static and dynamic stresses, thermal cycling and many other demanding loads [123]. Development of structural materials capable of withstanding these conditions is a major objective of many fusion development programs worldwide [3].

For the EU DEMO, the current baseline structural material is the Reduced Activation Ferritic Martensitic (RAFM) steel Eurofer97 [45]. RAFM steels, such as Eurofer97 were chosen over austenitic stainless steels due to their superior swelling resistance under irradiation, higher thermal conductivity and lower thermal expansion [6]. However, despite the relative maturity of RAFMs, their operating temperature range is somewhat narrow, being constrained by radiation embrittlement at low temperature and creep performance at high temperature,

giving a viable window of 325 – 550 °C [7]. For this reason, there have been ongoing attempts to develop superior alternatives to RAFM steels. One approach currently being explored is the use of nanoscale oxide particles to improve mechanical properties and radiation resistance. A key advantage of this strengthening mechanism is the thermal stability of the oxide particles, providing greater high temperature strength and creep performance [789]. While these Oxide Dispersion Strengthened (ODS) steels have shown significant promise, they are costly and time consuming to produce [7].

Separately, the development of high fluence neutron test facilities is underway to provide a more suitable environment in which to expose candidate materials e.g. the International Fusion Materials Irradiation Facility-DEMO Oriented Neutron Source (IFMIF-DONES) [4101112133]. However, the high flux irradiation volume in current designs will be somewhat limited (≤ 500 ml) [11131415]. Consequently, this has prompted significant interest in the use of subsize specimens and other small scale test techniques (SSTT) [131617]. SSTT is also of interest to the fission industry, since surveillance specimens have long been used in operating reactors to monitor material degradation [1819] and reducing the size of these is useful for both space, re-use (of larger tested specimens) and activation reasons [20].

^{*} Corresponding Author.

E-mail address: mark.richardson@ukaea.uk (M. Richardson).

<https://doi.org/10.1016/j.nme.2021.101067>

Received 12 May 2021; Received in revised form 23 August 2021; Accepted 31 August 2021

Available online 14 September 2021

2352-1791/Crown Copyright © 2021 Published by Elsevier Ltd. This is an open access article under the CC BY license (<http://creativecommons.org/licenses/by/4.0/>).

The small punch test is one such SSTT that has the potential to assess mechanical performance using reduced volumes of material. It also has the potential to accelerate alloy development by allowing the rapid assessment of small batches of novel alloys [21]. Given the limited production volume of ODS steels, they are an ideal candidate for assessment via such small sample testing techniques (SSTT). Small punch involves forcing a hemispherical punch or ball through a disk-shaped specimen under constant load (Small Punch Creep, SPC) or constant displacement rate [22,23]. The latter provides force–displacement data, while SPC can produce displacement–time curves, an example of which can be seen in Fig. 1. The standard dimensions for a small punch test specimen are a thickness of 0.5 mm and a diameter of 8 mm [24]. Given the small volume of material required, the test can be considered pseudo non-destructive, with techniques available for the in-situ removal of material from large components [22].

However, determining the mechanical properties (such as tensile and creep) of materials via small punch testing is still challenging due to the complex stress state that occurs during deformation [23,25]. Materials can be ranked by their relative performance [21], but require consistency in test methodology and data analysis to ensure reliability. Ongoing attempts at standardisation are intended to help address this [26,27], which will be critical if regulators are to accept the validity of SSTT data [28]. The new CEN small punch standard provides improved force-stress conversion methods [24], and related work has added to this with the Modified Chakrabarty (MCH) approach [29]. When estimating equivalent uniaxial stresses from small punch creep data, the MCH approach provides greater flexibility with regard to test setup [29]. This is particularly useful for comparing historic data that may not have been acquired in compliance with the current standard.

As mentioned earlier, ODS steels represent a promising alternative to the current baseline structural material for DEMO (Eurofer97), particularly the variant known as 14YWT [30]. This alloy contains nominally 14 wt% Cr, along with varying additions of W, Ti and Y_2O_3 [30]. Following initial development, various batches have been produced by different groups, including one at the University of Oxford, which was characterised in detail as part of an internal project [31]. This included microstructural analysis and assessment of time independent mechanical properties. However, there was insufficient time and resources to assess high temperature time dependent deformation i.e. creep behaviour. This paper therefore utilises SPC to assess the creep performance of this 14YWT batch and benchmarks it against the current baseline structural material for DEMO (Eurofer97). This includes determination of the force-stress conversion equations for a non-standard (1 mm radius punch) test setup using the recently developed MCH approach.

Materials and experimental method

The Eurofer97 used in this study was supplied by the Karlsruhe

Institute for Technology in the form of a 5 mm thick plate, produced by Bohler Bleche GMBH. After normalising at 980 °C, the plate was tempered at 760 °C for 90 min. The composition is detailed in Table 1. The ODS steel (14YWT) had a nominal composition, in wt%, of 14Cr, 3 W, 0.2Ti, 0.25 Y_2O_3 [31]. Fabrication was carried out using gas-atomised pre-alloyed powder (excluding Y_2O_3) supplied by Aubert & Duval. The oxide particles were introduced through the addition of Y_2O_3 during mechanical alloying (MA). This was performed using a Fritsch Pulverisette P5 planetary ball mill at 250 rpm for 60 h under an argon environment. To address contamination issues, milling pots and balls were custom made from AISI 50–100. The milling balls were 10 mm in diameter and a ball-to-powder weight ratio of 10:1 was employed. Consolidation was achieved through Hot Isostatic Pressing (HIP), carried out at 1150 °C under 150 MPa of pressure for a duration of four hours [31]. Table 1 illustrates the composition of the resulting product.

Characterisation of the starting microstructures was carried out through Electron Backscatter Diffraction (EBSD) using a TESCAN Field Emission Gun Scanning Electron Microscope (FEG SEM) for the Eurofer97 and a JEOL 6500F FEG SEM for the 14YWT. Due to the bimodal grain size of the 14YWT, multiple step sizes were used to characterise the microstructure at different length scales (0.1 μ m and 0.65 μ m for high and low magnification, respectively). The Eurofer97 could be adequately represented at an intermediate magnification with a step size of 0.11 μ m. Post-processing of the Eurofer97 EBSD data was carried out using Oxford Instruments HKL CHANNEL5 software [32], while the 14YWT had previously been analysed using EDAX Inc, TSL OIM software [31]. The Vickers hardness was ascertained using a Leco LM 100AT microhardness tester, with a 500 g load and a dwell time of 13 s. A minimum of 40 indents were made across specimens to provide a reliable average.

Fig. 1(a) illustrates the small punch setup employed in this study. Specimens 8 mm in diameter were removed from the as-received material through Electro-Discharge Machining (EDM), before wet grinding with SiC paper to reach their final thickness. The Eurofer97 specimens were oriented such that the flat face of each disk was parallel to the plane of the rolled plate (and therefore in the plane of the rolling direction). To remove the 14YWT specimens, a slice was first removed parallel to the axis of the HIPing can. Specimens were then machined in the plane of this slice. The final surface finish was achieved with p1200 grit SiC paper, to a target thickness of 0.5 mm \pm 1% (\pm 0.005 mm). While the majority of specimens conformed to this specification, a number of ‘over-thinned’ specimens (0.485 – 0.495 mm thick) were also tested. These are indicated in the results where included. Post-test microscopy of fracture surfaces in the present study was carried out with a TESCAN FEG SEM.

In accordance with the CEN Workshop Agreement (CWA 15627), a punch radius of 1 mm was used [22]. Testing was carried out using a servo-hydraulic rig with applied loads increasing in 75 N increments

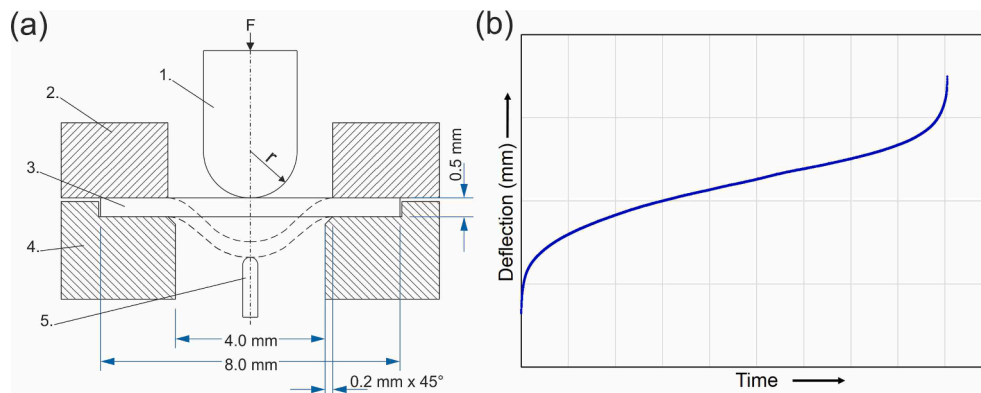


Fig. 1. (a) Small Punch Creep (SPC) test setup conforming to CWA 15,627 [22]; (1) Punch Head, (2) Clamping die, (3) Specimen, (4) Receiving Die, (5) Extensometer Rod, (b) illustrative small punch creep curve.

Table 1
Composition of 9Cr Eurofer97 plate and 14Cr ODS steel (14YWT) (wt%).

Alloy	ProductForm	Cr	W	Si	Mn	Ti	O	C	Y	Fe
Eurofer97	Plate	8.95	1.06	0.031	0.55	0.001	0.0007	0.11	–	Bal.
14YWT	HIP	13.34	2.81	–	0.38	0.22	0.23	0.08	0.19	Bal.

from 600 N to 825 N (with an extra 14YWT test at 630 N). These loads were chosen to evaluate the rapid testing capabilities of the SPC approach by maximising output. In benchmarking the ODS performance against Eurofer97, all tests were carried out at a temperature of 550 °C, in line with the expected upper operating temperature limit of Eurofer97 [6]. Loading was carried out at a rate of 2.5 N/s, while the time to reach load was excluded from time-to-failure data. Deformation was recorded via a ceramic rod in contact with the underside of the specimen, linked to an extensometer (see item 5 in Fig. 1(a)). In accordance with the draft standard, this extension measurement is referred to as ‘deflection’ (whereas ‘displacement’ refers to the position of the punch head tip) [2426]. While the 14YWT was tested under argon, the Eurofer97 was tested in air. To account for this variation, a separate study was carried out by Dawson et al to investigate the influence of environment on SPC testing of Eurofer97 [33]. Testing was undertaken at 675 N, corresponding to the mid-range of loads in the present study, and at which the most data points were acquired. Interpretation of the Eurofer97 results in Sections 3.2 and 4 are informed by the outcome of this investigation.

Force-Stress conversion methodologies

As mentioned earlier, SPC can readily provide a qualitative assessment of a material’s performance by ranking it against others [21]. However, for a more quantitative evaluation, some means of converting the SPC test load to an equivalent uniaxial stress is needed. What follows is a brief explanation of some existing methodologies, and the rationale behind using the Modified Chakrabarty (MCH) approach [29] in this study.

The central issue is that the stress state within a small punch specimen is a complex multiaxial one that changes throughout the test [2325]. This makes conversion of an SPC test load to a uniaxial equivalent stress somewhat difficult [23] and has hindered wider use of the technique [29]. However, among the ongoing efforts to standardise SPC are attempts to improve the analysis and interpretation of results [2926]. The original CEN Workshop Agreement 15,627 made use of analysis by Chakrabarty on stretch forming of circular blanks over hemispherical punch heads [22]. This approach ignores bending stresses and describes a biaxial stress state within a membrane stretched over a hemispherical punch [2234]. The equation derived takes the form:

$$\frac{F}{\sigma} = 2\pi \cdot h \cdot r \cdot \theta_0 \quad (1)$$

Where F is the applied load (N), σ is the equivalent stress (MPa), r is the punch radius (mm), θ_0 is the angle at the contact boundary (radians) and h is the disk thickness at the contact boundary (mm) (see Fig. 2(a)). The value of h can be found from:

$$h = h_0 \left\{ \frac{1 + \cos\theta_0}{1 + \cos\theta} \right\} \quad (2)$$

Where h_0 is the initial disk thickness (mm) and θ is the angle at the clamped boundary (see Fig. 2(a)). The relationship between θ and θ_0 is defined as follows:

$$\sin\theta = \frac{r}{R} \sin^2\theta_0 \quad (3)$$

Where R is the radius of the receiving aperture (mm) (see Fig. 2(a)). Chakrabarty also derived an expression for the central displacement of the punch, u_1 (or deflection, as in this case):

$$u_1 = R \sin\theta \ln \frac{\tan\left(\frac{\theta_0}{2}\right)}{\tan\left(\frac{\theta}{2}\right)} + r(1 - \cos\theta_0) \quad (4)$$

From Equations 1–4, F/σ can then be plotted as a function of deflection, see Fig. 2(b) (solid black line). It can be seen that the equivalent stress varies throughout a test, reaching a minimum at a deflection of approximately 1.4 mm (maximum F/σ). This is based on the specific test setup employed in this study ($r = 1$ mm). For the current standard setup ($r = 1.25$ mm), F/σ reaches a maximum at a deflection of 1.57 mm [29]. As explained in CWA 15627, regression analysis was then employed to produce a general formula based on the test setup parameters [22]:

$$\psi = \frac{F}{\sigma} = 3.33 \cdot k_{sp} \cdot R^{-0.2} \cdot r^{1.2} h_0 \quad (5)$$

Where k_{sp} is an SPC test correlation factor introduced to account for the variation in creep ductility between different materials, temperatures and stresses. Taking 1 as the default value for k_{sp} , the general formula provides an estimate of the stress based on the maximum F/σ ratio in the Chakrabarty curve. This value is independent of deflection,

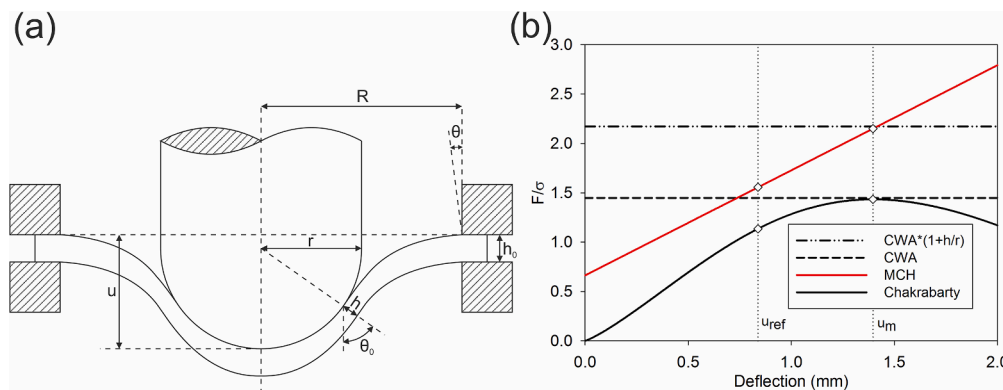


Fig. 2. (a) relevant parameters required for Chakrabarty’s membrane stretching model and (b) various force-stress conversion methodologies, including the original Chakrabarty approach [22], fitted equation from the CEN Workshop Agreement 15,627 (CWA) [22], a modified CWA approach ($CWA \cdot (1 + h_0/R)$) [29] and the Modified Chakrabarty (MCH) method adopted in this paper [29].

as illustrated by the dashed black line in Fig. 2(b). Since SPC tests may spend much of their duration outside the maximum F/σ state, the reliability of this method is highly dependent on the accuracy of k_{sp} . If good correlations with uniaxial data have been established, this should not be an issue. However, in the absence of such data, the reliability of any predicted stress will be limited [29]. Consequently, the new draft standard introduced a fully empirical deflection dependent model [2426]:

$$\Psi = \frac{F}{\sigma} = 1.9162 \cdot u_{min}^{0.6579} \quad (6)$$

Where u_{min} is the deflection at minimum deflection rate. Although this approach has been shown to reliably estimate equivalent uniaxial creep stresses in SPC tests [29], it applies specifically to the standard test setup ($r = 1.25$ mm) and may therefore be inaccurate in this case ($r = 1$ mm). However, Holmstrom et al have proposed a modified Chakrabarty (MCH) approach that can account for different test setups while retaining deflection dependence [29]. This is based upon the slope of the Chakrabarty curve at 60% of the deflection at which Ψ reaches its maximum (see Fig. 2(b)). The gradient is defined at 60% in order to mimic the curve of the empirical model in the draft standard [29] but will depend on the specific setup employed. The intercept is determined by passing the slope through a fixed point given by:

$$\Psi_{MCH(u_m)} = \frac{F}{\sigma} = (1 + h_0/r) \cdot \Psi_{cha(u_m)} \quad (7)$$

Where u_m is the deflection at maximum Ψ . This point is based on an estimation of the ultimate tensile strength of ductile materials [29]. Applying the MCH methodology to the setup used in this study ($r = 1$ mm, $R = 2$ mm), the following equation was determined for 0.5 mm thick specimens:

$$\Psi_{0.5mm} = 1.0649u_{min} + 0.6630 \quad (8)$$

Since the MCH approach accounts for h_0 , additional formulae were derived to incorporate non-standard specimens in the results (in this case, 0.485 mm and 0.49 mm thick):

$$\Psi_{0.485} = 1.0329u_{min} + 0.6223 \quad (9)$$

$$\Psi_{0.49} = 1.0436u_{min} + 0.6357 \quad (10)$$

One important factor not directly addressed here is that of friction between the punch and the specimen. Modelling and experiments have shown that friction can influence deformation behaviour during a small punch test [353637]. Although this is not directly accounted for in these analysis methodologies, the semi-empirical nature of the MCH approach may indirectly accommodate this to some extent.

Results

Microstructure and microhardness

Fig. 3 illustrates the starting microstructures, as imaged via EBSD. The bimodal grain size of the ODS steel required imaging at both high and low magnification, whereas the Eurofer97 could be adequately represented at an intermediate magnification. Fig. 3(a) illustrates the Eurofer97 microstructure through Inverse Pole Figure (IPF) colouring of the ferrite phase, with a reference axis perpendicular to the plane of the EBSD map. The apparent lack of martensite may be due to the similarity in lattice parameters preventing the acquisition software from distinguishing between the two phases. The original map contained 91.27% successfully indexed points/pixels. To facilitate more reliable grain size analysis, noise in the data was reduced by removing wild spikes and using the nearest neighbours to each zero solution (iterating from eight down to three nearest neighbours). Grain size was determined via post-processing software using the equivalent circular diameter method. A lower limit of three pixels per grain was set and boundaries were defined by a minimum misorientation of 5° . With these parameters, the mean grain diameter of the Eurofer97 was found to be $1.3 \mu\text{m}$.

Fig. 3(b) illustrates the 14YWT microstructure at low magnification. The black regions indicate areas where the grain structure was too fine to be indexed reliably. Consequently, these were mapped at higher resolution to reveal the finer microstructure, as shown in Fig. 3(c). Using the same parameters as above, the mean grain diameter was found to be $4.3 \mu\text{m}$ at low magnification and 300 nm in the finer regions [31]. From the hardness tests, the Eurofer97 was found to have a Vicker's hardness of $227 \text{ HV} \pm 1$ (95% confidence limit). However, the hardness value of the 14YWT ODS steel was considerably higher, at $435 \text{ HV} \pm 4$.

Small punch creep behaviour

Fig. 4 illustrates the time to failure of Eurofer97 and 14YWT as a function of load at 550°C . Unfortunately, data from specimens conforming to the thickness tolerance of 1% were unavailable for the 14YWT at 750 N. However, it can still be seen that the 14YWT ODS steel outperforms the Eurofer97. The investigation by Dawson et al revealed that testing under argon could increase the time to failure and deflection at failure of Eurofer97 by up to 30% and 7%, respectively [33]. No significant effect was observed on the minimum deflection rate [33]. To illustrate the potential effect of this on the Eurofer97 data in this study, a correction has been applied in Fig. 4. The solid blue line is fitted to the actual (in air) data, while the blue dashed line has been shifted by 30% to reflect the maximum effect of testing in argon. It can be seen that the 14YWT still retains a significant advantage over the Eurofer97. This

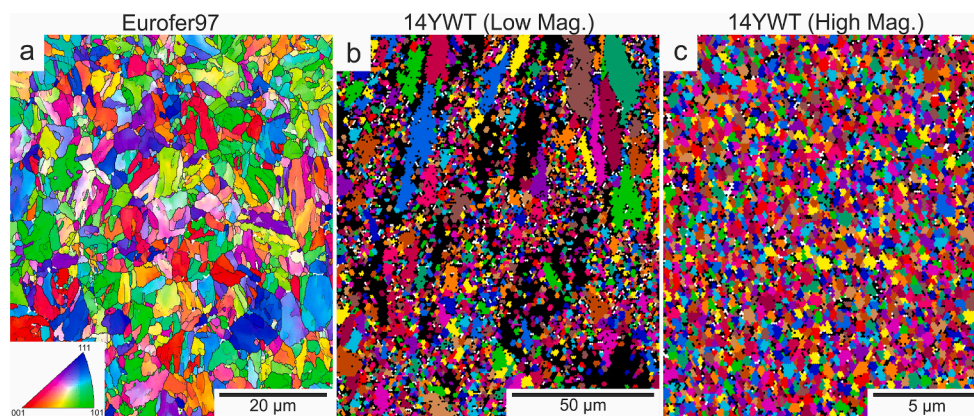


Fig. 3. EBSD maps of as-received microstructures, illustrating (a) Eurofer97 plate under Inverse Pole Figure (IPF) colouring and (b)-(c) the bimodal microstructure of 14YWT ODS steel under unique grain colouring [31]. Reference axis for (a) is perpendicular to the plane of the map.

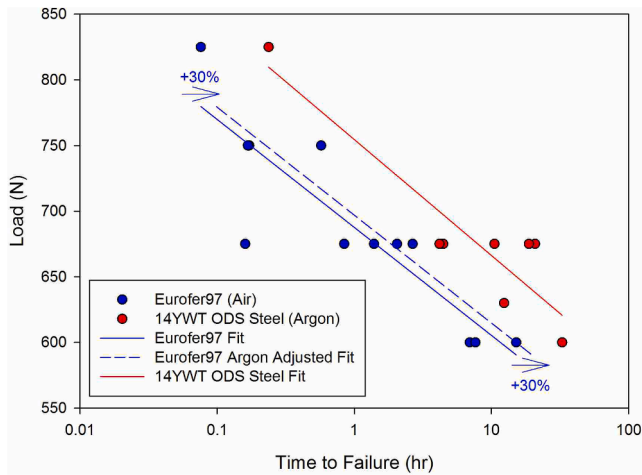


Fig. 4. Small Punch Load-Time to failure comparison of Eurofer97 and 14YWT ODS steel at 550 °C, including adjusted Eurofer97 curve to account for differing test environments [33] (Eurofer97 in air, 14YWT ODS steel under argon).

difference is reflected in the minimum deflection rate, illustrated in Fig. 5 as a function of load. Both materials also adhere to the Monkman-Grant relationship between minimum deflection rate and time-to-failure, see Fig. 6 [38]. Although the draft standard includes an equation for converting between minimum deflection rate and minimum uniaxial strain rate, this was empirically derived from the standard test set-up (i.e. a punch radius of 1.25 mm) and is therefore inapplicable here (where a punch radius of 1 mm was used) [2426]. However, the validity of the Monkman-Grant relationship should lend confidence to the predictability of material behaviour.

Representative secondary electron (SE) micrographs of fracture surfaces are presented in Fig. 7. Both Eurofer97 and the 14YWT produced ‘caps’ that separated from the specimens at failure, as is typical of small punch tests of ductile materials [29]. However, it can be seen that the ODS steel also experienced significant radial cracking, suggesting that it has lower ductility than the Eurofer97. This is supported by the lower deflection at failure of 14YWT (Fig. 8(a)), which also appears stiffer, in that it exhibits lower deflection under initial loading (Fig. 8 (b)).

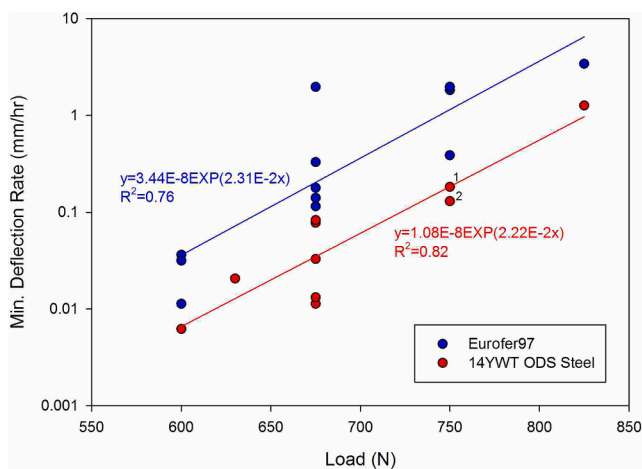


Fig. 5. Minimum deflection rate of Eurofer97 and 14YWT ODS steel as a function of load, during small punch creep testing at 550 °C. Numbered specimens are outside specification: 1 (0.485 mm thick), 2 (0.49 mm thick).

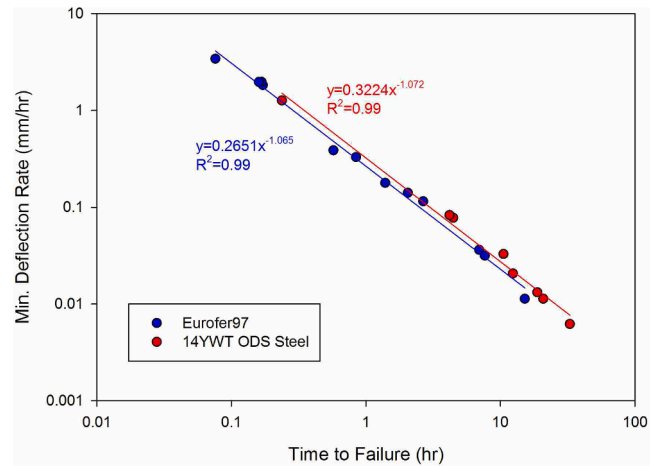


Fig. 6. Minimum deflection rate vs time to failure of Eurofer97 and 14YWT ODS Steel at 550 °C, illustrating the Monkman-Grant relationship.

Discussion

The superior time-to-failure data of the 14YWT relative to Eurofer97 is not unexpected in light of the oxide dispersion strengthening [7]. The presence of a high number density (approx. $2.4 \times 10^{23} \text{ m}^{-3}$) of randomly distributed Y, Ti and O rich precipitates, on the order of 2–5 nm in diameter was confirmed by Gorley [31] via Atom Probe Tomography. This strengthening is also reflected in the much higher room temperature hardness of the 14YWT (435 HV vs 227 HV), although the thermal stability of oxide particles is less pertinent at such temperatures [89]. Additional hardening mechanisms may also contribute to the higher strength of the 14YWT e.g. the fine grained regions of the microstructure shown in Fig. 3(c). However, as Figs. 7 and 8 illustrate, the higher strength and time-to-failure performance may come at the expense of ductility. Again, this is not unexpected as strength and ductility are often inversely correlated [39]. However, that isn't to say further microstructural optimisation isn't possible. The bimodal grain size may be one aspect of the microstructure that could improve ductility through careful modification [4041].

Although the grain size of the Eurofer97 appears relatively uniform in Fig. 3(a), it was noted by the supplier that there was some non-uniformity within the microstructure, with large grains distributed sporadically throughout. This may explain some of the scatter observed in the Eurofer97 data. While some scatter is to be expected in creep data, and small punch adds a further layer of variation to this, it is unusual that the more ductile material (Eurofer97) exhibits more scatter than the less ductile material (14YWT), as in Fig. 5. In addition, further fluctuations may be induced by through-thickness microstructural variation in the as-received plate.

Referring to Fig. 8(a), the total deflection (deflection at failure) is shown to be relatively uniform across all loads for Eurofer97 ($\approx 1.6 \text{ mm}$), whereas the total deflection of 14YWT appears to vary linearly with test load, ranging from around 0.8 mm (600 N) to approximately 1.25 mm (825 N). The cause of this load dependence is unclear. One possibility is that a change of deformation mode is occurring. Given the relatively short duration of these SPC tests (i.e. relatively high load), it may be that they straddle the boundary between diffusional and dislocation based deformation processes. At high loads, dislocation processes are expected to dominate [42], giving rise to a more ductile, transgranular fracture, whereas at lower loads, a more brittle, intergranular fracture is expected [4344].

Thus far, the performance of Eurofer97 and 14YWT have only been compared in relative terms. Therefore, using the MCH approach described in Section 2.1, the test loads were converted to estimated uniaxial equivalent stresses, and the revised data is presented in Fig. 9

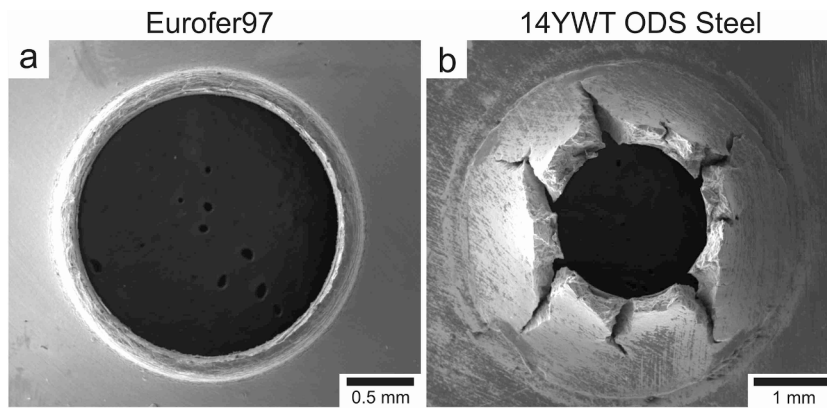


Fig. 7. SE micrographs of small punch creep specimens tested at 550 °C.

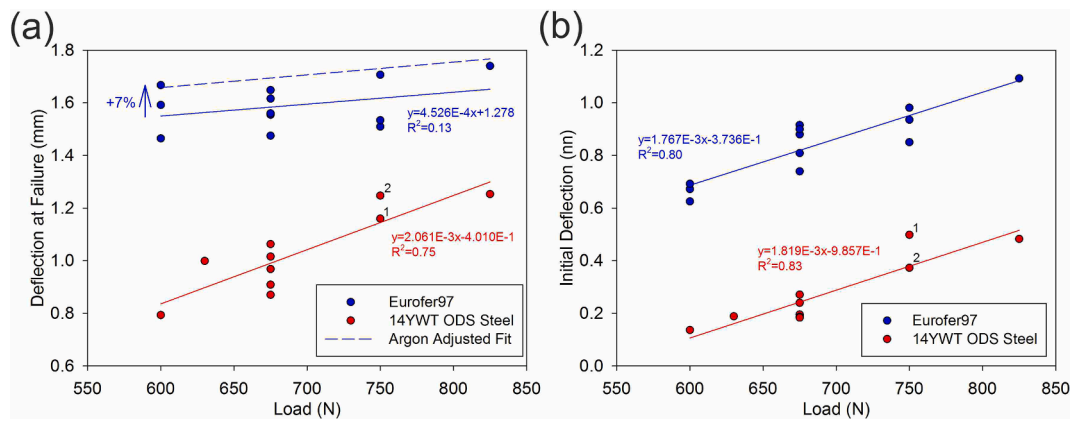


Fig. 8. Variation in deflection throughout small punch creep testing of Eurofer97 and 14YWT ODS steel at 550 °C, illustrating (a) deflection at failure (total deflection), and (b) initial loading induced deflection (time independent deformation). Numbered specimens are outside specification: 1 (0.485 mm thick), 2 (0.49 mm thick) (fitted lines incorporate these data points). Eurofer97 equation applies to unadjusted (in air) data.

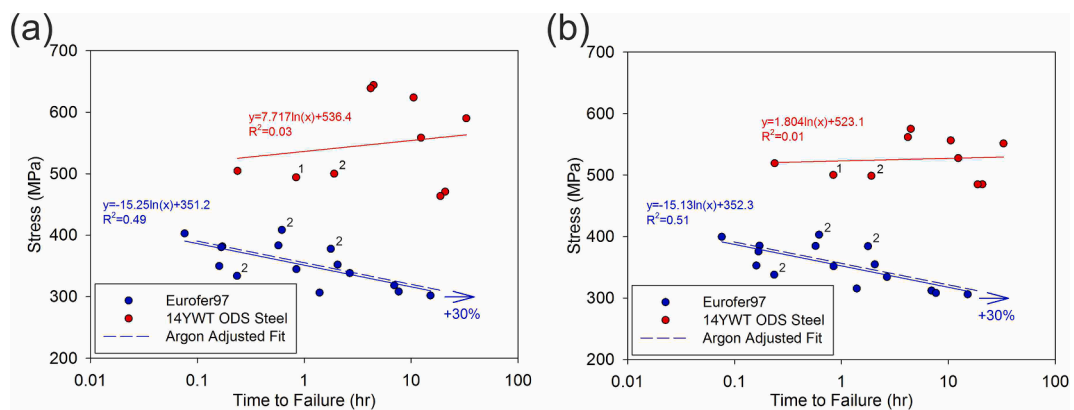


Fig. 9. Estimated equivalent uniaxial stress vs time to failure comparison of Eurofer97 and 14YWT ODS steel at 550 °C. Force-stress conversion based on (a) deflection at minimum deflection rate, and (b) deflection at half rupture time. Numbered specimens are outside specification (including additional Eurofer97 data): 1 (0.485 mm thick), 2 (0.49 mm thick) (fitted lines apply to unadjusted (in air) data).

(a). While the 14YWT appears to retain its superior performance relative to Eurofer97, a significant amount of scatter is introduced, and the expected relationship between stress and time-to-failure breaks down. This raises doubts over the accuracy of the 14YWT estimated stress values. While the Eurofer97 data also exhibited an increase in scatter, the trend is still reasonable. The irregular effect of the force-stress conversion process on the 14YWT may be related to its relatively low ductility. As pointed out in CWA 15627, the Chakrabarty analysis is not valid at low

strains, as the bending moment is ignored and F/σ approaches zero (i.e. membrane stresses tend to infinity) [22]. As Fig. 8 illustrated, the 14YWT failed at significantly lower deflections than the Eurofer97, possibly compromising the accuracy of the stress estimates.

Another potential issue is the determination of u_{min} . As illustrated in Fig. 10, the deflection rate of Eurofer97 reaches a more obvious minima than 14YWT, and may therefore provide a more consistent deflection from which to estimate equivalent stress. The deflection rate of 14YWT

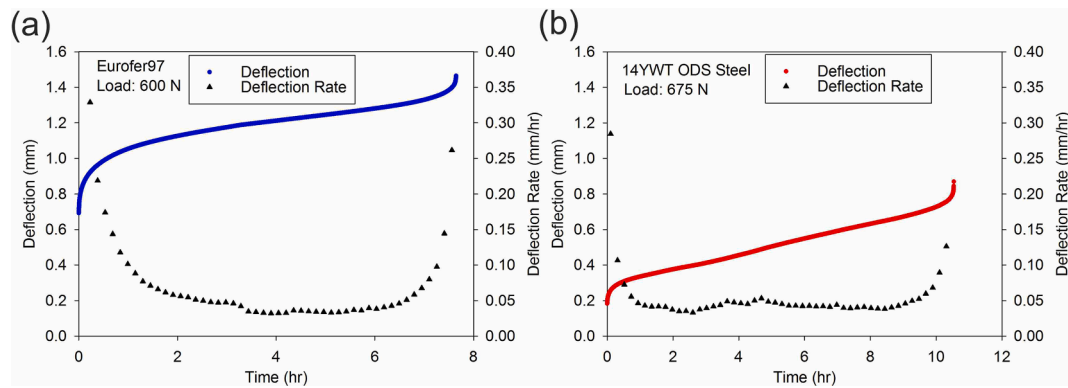


Fig. 10. Representative deflection and deflection rate curves of Eurofer97 and 14YW7 ODS steel at 550 °C under (a) 600 N and (b) 675 N.

'levels off' more clearly, but this may actually introduce more scatter in u_{min} , as smaller variations in the deflection rate will shift u_{min} more dramatically. In addition, issues with data acquisition and smoothing can further complicate the determination of u_{min} . These problems were encountered in the development of MCH, and led to suggestions that a more consistent option might be the use of deflection at $1/2t_r$ (half rupture time) [29]. To assess the effect of such a methodology, the data was re-evaluated based on $1/2t_r$, and is presented in Fig. 9(b). The Eurofer97 data appears almost unchanged. However, although the 14YW7 scatter may have reduced slightly, there is still no reliable trend.

The deflection dependence of the MCH approach is intended to compensate for the variation in equivalent stress that occurs throughout an SPC test. Within the deflection range of most tests, Chakrabarty's analysis shows the membrane stress falling as deflection rises, see Fig. 2 (b). Lower load tests (which spend longer at lower deflections) may therefore be subjected to higher equivalent stress than expected, which the MCH model adjusts for. However, if there is overcompensation, this might lead to overestimation of the stresses in lower load (i.e. longer duration) tests and vice versa, thus 'flattening' the trendline in stress-time to failure data. As illustrated in Fig. 8, the 14YW7 exhibited significantly more variation in total deflection (deflection at failure) than the Eurofer97. Consequently, there was much greater variation in the deflection values used to estimate equivalent stresses. This behaviour might be responsible for the erratic force-stress conversion results of the 14YW7, and may render it unsuitable for analysis by MCH. However, under equivalent loads, ODS 14YW7 has nevertheless demonstrated superior performance as a high temperature, creep resistant alloy, relative to Eurofer97.

Conclusions

This study assessed the small punch creep properties of Eurofer97 and a 14YW7 ODS steel at 550 °C. The 14YW7 demonstrated superior time-to-failure and significantly lower rates of deformation. However, it also suffered reduced ductility and exhibited a mixed mode failure. The Modified Chakrabarty (MCH) approach was employed to estimate equivalent uniaxial creep stresses. While the conversion was relatively smooth for Eurofer97, it introduced a significant amount of scatter in the 14YW7 data. Since the MCH method assumes membrane stretching behaviour, the low ductility of 14YW7 may have been responsible for the erratic force-stress conversion results. Further work is needed to identify the limits of existing models and, where necessary, develop models for materials with reduced ductility. These issues made accurate estimation of the 14YW7 performance difficult, but did not undermine the conclusion that it possessed superior creep resistance, in terms of both time-to-failure and dimensional stability (a key concern of designers). However, given the relatively high load (short duration) regime of the testing, care should be exercised in extrapolating from this to longer timescales, as the dominant deformation mode is likely to

change.

CRediT authorship contribution statement

M. Richardson: Conceptualization, Project administration, Methodology, Investigation, Writing - original draft, Writing - review & editing. **M. Gorley:** Conceptualization, Project administration, Methodology, Investigation, Writing - review & editing. **Y. Wang:** Conceptualization, Writing - review & editing. **D. Andres:** Methodology, Writing - review & editing. **H. Dawson:** Methodology, Investigation, Writing - review & editing.

Declaration of Competing Interest

The authors declare that they have no known competing financial interests or personal relationships that could have appeared to influence the work reported in this paper.

Acknowledgements

This work has been funded by the RCUK Energy Programme [grant number EP/T012250/1. To obtain further information on the data and models underlying this paper please contact PublicationsManager@ukaea.uk.

This research made use of the UKAEA's Materials Research Facility, which has been funded by and is part of the UK's National Nuclear User Facility and Henry Royce Institute for Advanced Materials.

The authors also wish to thank the Karlsruhe Institute of Technology for supply of the Eurofer97 rolled plate.

References

- [1] I. T. Chapman and A. W. Morris, "UKAEA capabilities to address the challenges on the path to delivering fusion power," *Philos. Trans. R. Soc. A Math. Phys. Eng. Sci.*, vol. 377, no. 2141, 2019.
- [2] E. Surrey, "Engineering challenges for accelerated fusion demonstrators," *Philos. Trans. R. Soc. A Math. Phys. Eng. Sci.*, vol. 377, no. 2141, 2019.
- [3] D. Stork and S. J. Zinkle, "Introduction to the special issue on the technical status of materials for a fusion reactor," *IOP*, vol. 57, 2017.
- [4] D. Stork, et al., *Materials R&D for a timely DEMO: Key findings and recommendations of the EU Roadmap Materials Assessment Group*, *Fusion Eng. Des.* 89 (7–8) (2014) 1586–1594.
- [5] D. Stork, et al., *Assessment of the EU R&D Programme on DEMO Structural and High-Heat Flux Materials*, *EUROfusion* (2012).
- [6] H. Tanigawa et al., "Development of benchmark reduced activation ferritic/martensitic steels for fusion energy applications," *Nucl. Fusion*, vol. 57, no. 9, 2017.
- [7] S. J. Zinkle et al., "Development of next generation tempered and ODS reduced activation ferritic/martensitic steels for fusion energy applications," *Nucl. Fusion*, vol. 57, no. 9, 2017.
- [8] M. J. Alinger, G. R. Odette, and D. T. Hoelzer, "The development and stability of Y-Ti-O nanoclusters in mechanically alloyed Fe-Cr based ferritic alloys," *J. Nucl. Mater.*, vol. 329–333, no. 1–3 PART A, pp. 382–386, 2004.

- [9] S.Y. Zhong, J. Ribis, V. Klosek, Y. de Carlan, N. Lochet, V. Ji, M.H. Mathon, Study of the thermal stability of nanoparticle distributions in an oxide dispersion strengthened (ODS) ferritic alloys, *J. Nucl. Mater.* 428 (1-3) (2012) 154–159.
- [10] D. Stork, P. Agostini, J.L. Boutard, D. Buckthorpe, E. Diegele, S.L. Dudarev, C. English, G. Federici, M.R. Gilbert, S. Gonzalez, A. Ibarra, C.h. Linsmeier, A. Li Puma, G. Marbach, P.F. Morris, L.W. Packer, B. Raj, M. Rieth, M.Q. Tran, D. J. Ward, S.J. Zinkle, Developing structural, high-heat flux and plasma facing materials for a near-term DEMO fusion power plant: The EU assessment, *J. Nucl. Mater.* 455 (1-3) (2014) 277–291.
- [11] A. Ibarra F. Arbeiter D. Bernardi M. Cappelli A. García R. Heidinger W. Krolas U. Fischer F. Martin-Fuertes G. Micciché A. Muñoz F.S. Nitti M. Pérez T. Pinna K. Tian 58 10 2018 105002 10.1088/1741-4326/aad91f.
- [12] A. Ibarra, “IFMIF-DONES progress and future plans,” pp. 1–35, 2019.
- [13] F. Arbeiter et al., “Planned material irradiation capabilities of IFMIF-DONES,” *Nucl. Mater. Energy*, vol. 16, no. December 2017, pp. 245–248, 2018.
- [14] F. Arbeiter, A. Abou-Sena, J. Averhals, T. Böttcher, Y. Chen, B. Dolensky, U. Fischer, A. Heinzl, V. Heinzl, T. Heupel, P. Jacquet, C.h. Klein, A. Klis, K. Kondo, J. Konrad, R. Lindau, A. Möslang, A. Mucche, H. Piecha, R. Rolli, G. Schlindwein, P. Schubert, F. Schwab, K. Zinn, Design description and validation results for the IFMIF High Flux Test Module as outcome of the EVEDA phase, *Nucl. Mater. Energy* 9 (2016) 59–65.
- [15] T. Yokomine, S. Ebara, A. Shimizu, Thermo-hydraulic design of high flux test module for ifmif-evEDA in Japan, *Fusion Sci. Technol.* 56 (1) (2009) 267–272.
- [16] P. Jung, A. Hishinuma, G.E. Lucas, H. Ullmaier, Recommendation of miniaturized techniques for mechanical testing of fusion materials in an intense neutron source, *J. Nucl. Mater.* 232 (2-3) (1996) 186–205.
- [17] B. Giannone et al., “IFMIF Comprehensive Design Report,” p. 138, 2004.
- [18] J. Knaster et al., “Overview of the IFMIF / EVEDA project,” 2017.
- [19] D. Stork et al., “Towards a programme of testing and qualification for structural and plasma-facing materials in ‘fusion neutron’ environments,” *Nucl. Fusion*, vol. 57, no. 9, 2017.
- [20] M. Kapušňák, J. Petzová, M. Březina, M. Adamech, Interim results of the reactor pressure vessel materials evaluation within the framework of the implemented Advanced Surveillance Specimen Programme, in: in *Proceedings of the 5th International Small Sample Test Techniques Conference*, 2018, pp. 58–66.
- [21] R.J. Lancaster, S.P. Jeffs, in: *Creep*, InTech, 2018, <https://doi.org/10.5772/intechopen.70375>.
- [22] CEN, “CWA, 15627: Small Punch Test Method for Metallic Materials” 2007 CEN, Brussels.
- [23] M. Bruchhausen, S. Holmström, I. Simonovski, T. Austin, J.-M. Lapetite, S. Ripplinger, F. de Haan, Recent developments in small punch testing: Tensile properties and DBTT, *Theor. Appl. Fract. Mech.* 86 (2016) 2–10.
- [24] “BS EN 10371:2021 Metallic Materials. Small punch test method.” BSI, 2021.
- [25] A. Janča, J. Siegl, P. Hausild, Small punch test evaluation methods for material characterisation, *J. Nucl. Mater.* 481 (2016) 201–213.
- [26] M. Bruchhausen, et al., European standard on small punch testing of metallic materials, in: in *Proceedings of the 5th International Small Sample Test Techniques Conference*, 2018, pp. 1–14.
- [27] R. Kopriva, M. Brumovsky, P. Petelova, Current status of the small punch test standardization within the ASTM, in: in *Proceedings of the 5th International Small Sample Test Techniques Conference*, 2018, pp. 26–30.
- [28] A. Morris, B. Cacciapuoti, W. Sun, The role of small specimen creep testing within a life assessment framework for high temperature power plant, *Int. Mater. Rev.* 63 (2) (2018) 102–137.
- [29] S. Holmström, Y. Li, P. Dymacek, E. Vacchieri, S.P. Jeffs, R.J. Lancaster, D. Omacht, Z. Kubon, E. Anelli, J. Rantala, A. Tonti, S. Komazaki, Naveena, M. Bruchhausen, R.C. Hurst, P. Hähner, M. Richardson, D. Andres, Creep strength and minimum strain rate estimation from Small Punch Creep tests, *Mater. Sci. Eng. A* 731 (2018) 161–172.
- [30] D. T. Hoelzer, J. Bentley, M. A. Sokolov, M. K. Miller, G. R. Odette, and M. J. Alinger, “Influence of particle dispersions on the high-temperature strength of ferritic alloys,” *J. Nucl. Mater.*, vol. 367-370 A, no. SPEC. ISS., pp. 166–172, 2007.
- [31] M. J. Gorley, “Powder processing of oxide dispersion strengthened alloys for nuclear applications,” 2014.
- [32] M. D. Richardson S. Connolly M. Gorley B. P. Wynne E. Surrey 48 2 2020 20180619 10.1520/JTE2003-EB 10.1520/JTE20180619.
- [33] H. Dawson, M. Richardson, M. Gorley, and S. E., “The effect of testing environment on small punch creep,” in *Proceedings of the 5th International Small Sample Test Techniques Conference*, 2018, pp. 359–369.
- [34] J. Chakrabarty, A theory of stretch forming over hemispherical punch heads, *Int. J. Mech. Sci.* 12 (4) (1970) 315–325.
- [35] T. Nakata, S.-ichi. Komazaki, Y. Kohno, H. Tanigawa, Development of a small punch testing method to evaluate the creep property of high Cr ferritic steel: Part II - Stress analysis of small punch test specimen by finite element method, *Mater. Sci. Eng. A* 666 (2016) 80–87.
- [36] T. Nakata, S.-ichi. Komazaki, Y. Kohno, H. Tanigawa, Development of a small punch testing method to evaluate the creep property of high Cr ferritic steel: Part I - Effect of atmosphere on creep deformation behavior, *Mater. Sci. Eng. A* 666 (2016) 54–60.
- [37] R.V. Prakash, S. Arunkumar, Influence of Friction on the Response of Small Punch Test, *Trans. Indian Inst. Met.* 69 (2) (2016) 617–622.
- [38] F.C. Monkman, N.J. Grant, An Empirical Relationship Between Rupture Life and Minimum Creep Rate in Creep-Rupture Tests, *ASTM Proceedings* 1956 (1956) 593–620.
- [39] Yujie Wei Yongqiang Li Lianchun Zhu Yao Liu Xianqi Lei Gang Wang Yanxin Wu Zhenli Mi Jiabin Liu Hongtao Wang Huajian Gao 5 1 2014 10.1038/ncomms4580.
- [40] A.P. Gulyaev, L.N. Serebrennikov, Effect of differences in grain size on the mechanical properties of steel 18Kh2N4MA, *Met. Sci. Heat Treat.* 19 (4) (1977) 253–256.
- [41] Z. Dapeng, L. Yong, L. Feng, W. Yuren, Z. Liujie, D. Yuhai, ODS ferritic steel engineered with bimodal grain size for high strength and ductility, *Mater. Lett.* 65 (11) (2011) 1672–1674.
- [42] N.E. Dowling, *Mechanical Behavior of Materials*, 4th ed., Pearson, Harlow, 2013.
- [43] G.S. Deshmukh, M.L. Prasad, D.R. Peshwe, J. Ganesh Kumar, M.D. Mathew, G. Amarendra, Creep Properties Assessment of P92 Steel by Small Punch Creep Tests, *Trans. Indian Inst. Met.* 69 (2016) 907–915.
- [44] K. Maruyama, Fracture mechanism map and fundamental aspects of creep fracture, in: F. Abe, K. Torstern-Ulf, R. Viswanathan (Eds.), *Creep-Resistant Steels*, Woodhead Publishing Ltd., Cambridge, 2008, pp. 350–364.